Front. Phys. 12(5), 125201 (2017)
DOI 10.1007/s11467-017-0676-8

RESEARCH ARTICLE

Coherent resonance of quantum plasmons in Stone–Wales defected graphene–silver nanowire hybrid system

Tong Liu (刘彤)[1], **Hong Zhang** (张红)[1,2,†], **Xin-Lu Cheng** (程新路)[2], **Yang Xu** (徐阳)[1]

[1] *College of Physical Science and Technology, Sichuan University, Chengdu 610064, China*
[2] *Key Laboratory of High Energy Density Physics and Technology of Ministry of Education, Sichuan University, Chengdu 610064, China*
Corresponding author. E-mail: [†] *hongzhang@scu.edu.cn*
Received September 2, 2016; accepted January 25, 2017

Defected graphene has a more important practical significance than graphene. Silver nanoparticles can modify the optical properties of defected graphene. We present herein a detailed theoretical analysis about the coherent resonance of quantum plasmons in the Stone–Wales (SW) defected graphene–silver nanowire hybrid system by using time-dependent density functional theory. The plasmon coherent effect is mainly attributed to the electromagnetic field coupling between the Stone–Wales defected graphene and silver nanowires. As a result, the optical response of the hybrid system exhibits a remarkable enhancement. Plasmon resonance, which depends on polarization and selectable tuning, is enhanced in wide frequency regions. Moreover, it reveals that the resonance frequency of an optical absorption spectrum depends on the space configuration of the SW defected graphene in the hybrid system. This investigation provides a better understanding of the plasmon enhancement effect used in a graphene-based photoelectric device. The study also offers an effective means of detecting the defects existing in graphene.

Keywords quantum plasmons, coherent resonance, SW defected graphene, silver nanowires, hybrid system

PACS numbers 52.40.Fd, 52.27.Gr, 73.22.-f

1 Introduction

Surface plasmons (SPs) that are usually found in noble metal nanostructures have collective excitation, which offers opportunities of breaking the diffraction limit at a nanoscale [1, 2]. SPs have potential applications in a wide range, such as in optical biosensors [3], optical waveguides [4], optical nanoantennas [5], and quantum information processing [6]. Previous studies found that plasmon optoelectronic devices are produced by traditional metal nanometer materials, such as gold, silver, copper, and aluminum, among others. However, SPs also pose problems, with their main issue being their signal making a very severe attenuation during transmission. Graphene is one of the most fascinating two-dimensional materials with a planar honeycomb monolayer of carbon atoms [7]. Graphene has emerged as a very promising plasmonic material [8–13] because of its high carrier mobility [14], long mean free path, low scattering, and gate-tunable carrier densities [15]. In this context, combining graphene with plasmon materials, such as noble metals, to form a hybrid structure is an effective method of extending the frequency of plasmons from the ultraviolet region to the infrared and visible region [16]. Recent optical experiments demonstrated metal nanostructures as an optical frequency antenna, which can effectively capture light energy into the electromagnetic energy [17–20].

However, obtaining perfect graphene during preparation is almost impossible because of the limitation of the manufacturing process. All sorts of defects in graphene inevitably appear. In addition, graphene properties are susceptible to micro internal defects, including SW, vacancy, adsorption, and 5–8 pair defects. As one kind of topological defect, the SW defect is the most common defect existing in graphene, which forms when the

Frontiers of Physics

C–C key rotates for 90° along the key centers and the original complete hexagon forms two pentagons and a heptagon structure (Fig. 1). This type of defects was discovered by T. Ebbesen. Once formed, a 5–7 member ring would move in the structure and lead the structure to restructure a large area and destroy the integrity of graphene [21]. Moreover, the attention on the SW defected graphene is relatively weaker than on graphene, and theoretical and experimental research about plasmons is deficient. Therefore, a theoretical research on plasmons as regards the defects in graphene, especially the SW defect, has an important guiding significance for the practical application of graphene.

The plasmon characteristics from metal particles and graphene in the hybrid structure cause great change because of the electromagnetic coupling between graphene and metal particles. This changed leads to some novel optical effects [22–26]. The resonance frequency can be tuned by size [27, 28], shape [29], surrounding medium [30, 31], and excitation [32, 33] (polarization and propagation directions). It also makes a certain indicative to the superiority of the coupling structure comprising SW defected graphene and noble metal nanoparticles. However, we also need to study the micro process of plasmon at an atomic level to grasp the enhancement mechanism of plasmon in the hybrid structure. In the experiment, self-assembly techniques through the surface or the scanning tunneling microscope (STM) tip can be used to realize the manipulation of individual atoms in the material surface to form a variety of man-made atomic structure by Refs. [34–37]. In the process of actual operation , combines microscale SW defected graphene and metal particles to form the coupling structure has the realizability. At the same time, the quantum effect is leading to some novel phenomena along with the optical device being continuously developed in the molecular and nanoscale direction. Recognizing only the micromechanism of physical phenomena, we can control the graphene plasmon by reasonable means and provide a direct theoretical support for the application of a graphene nano-optoelectronic device.

In this letter, we mainly use the time-dependent density functional theory to obtain the numerical simulation of plasmons in a hybrid structure consisting of small-scale SW defected graphene with silver nanowires. This artificial atomic structure is an ideal candidate structure for merging the properties with the nanoscale SW defected graphene in a planar device. Compared with isolated SW defected graphene, the simple hybrid structure exhibits a remarkable enhancement on optical response. The optical absorption intensity and the resonance frequency are proportional to the nanowire length. These simulation results may offer essential information for controlling plasmons in an ultra-small practical graphene device. Furthermore, the results provide a viable means for detecting defects in graphene.

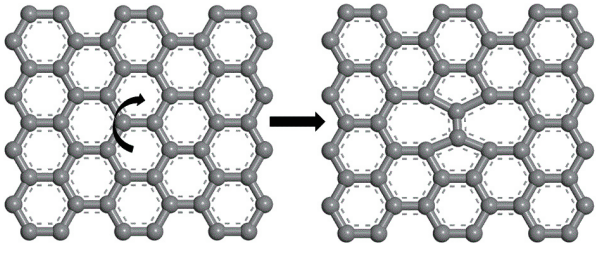

Fig. 1 Formation of Stone–Wales defects in graphene.

2 Computational details

All our calculations were performed using the real-space and real-time time-dependent density functional theory (TDDFT) approach, as employed in the OCTOPUS code [38]. All atoms were described by Troullier–Martins pseudopotentials [39]. The local density approximation [40] for the exchange correlation was used in both the ground and excited state calculations following Marinopoulos *et al.* The system is excited by a function impulse in the initial state to obtain the linear optical absorption spectrum. At the same time, we could also obtain a response to a particular polarization. The excitation spectra were extracted by Fourier transform of the dipole strength. This scheme was extensively tested on several well-studied examples to reproduce reliable absorption spectra [41, 42]. The simulation zone was a sphere around each atom with a radius of 6 Å and a uniform mesh grid of 0.2 Å. In a real-time propagation, the Kohn–Sham wave functions are evolved for typically 6000 steps with a time step of $\Delta t = 0.003\ \hbar/\mathrm{eV}$.

3 Results and discussion

We first mainly considered a series of hybrid structures by placing a rectangular SW defected graphene flake in the gap of a small silver nanowire dimer with planar structures. Figure 2 shows that a series of optical absorption spectrum of SW defected graphene with different lengths of silver nanowire hybrid structure and excitation pulse polarize along the zigzag edge of the SW defected graphene (parallel to the X axis). The distance between the edge of the SW defected graphene and the nearest Ag atom was 2.6 Å. The theoretical calculation model was a nonperiodic structure. The theoretical studies of the localized surface plasmon herein were in a small-scale nanostructure. For an intuitive comparison, Fig. 2 also illustrates the optical absorption spectrum

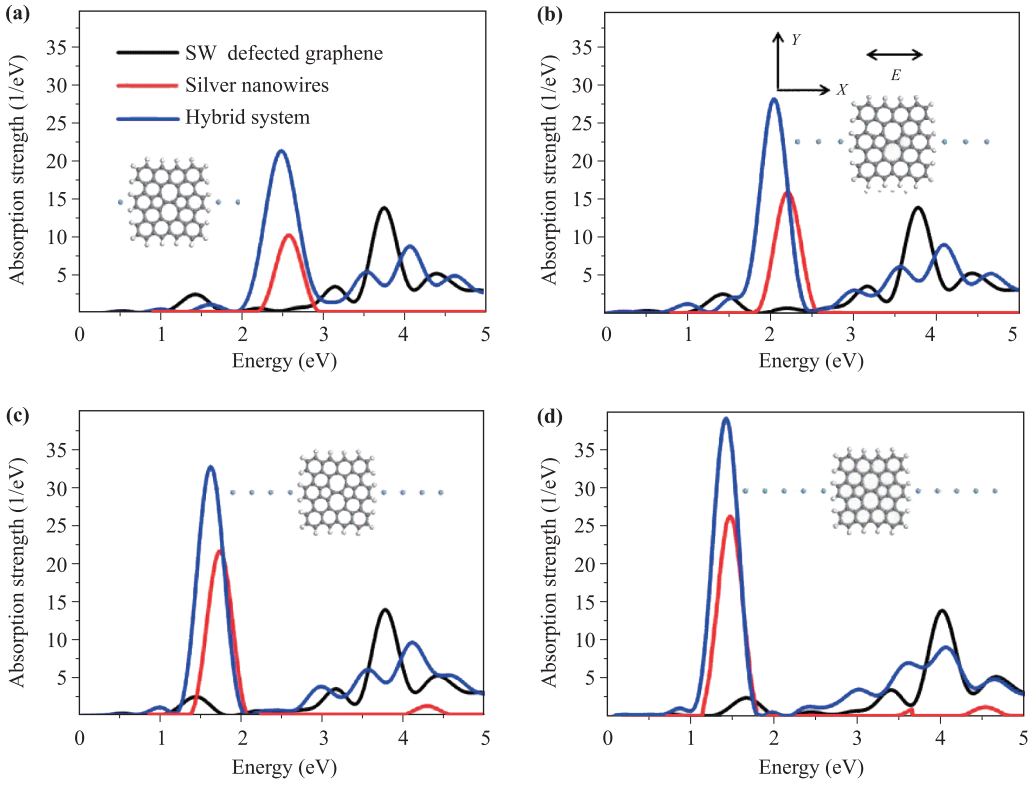

Fig. 2 Absorption spectra of a series of SW defected graphene–silver nanowires hybrid structures consisting of same SW defected graphene and variable silver nanowires: **(a)** Ag2 dimer, **(b)** Ag3 dimer, **(c)** Ag4 dimer, and **(d)** Ag5 dimer, respectively.

for the isolated SW defected graphene (black curve), isolated silver nanowires (red curve), and hybrid system (blue curve). The flake of the SW defected graphene at nanoscale splits into several discrete models because of the quantum confinement effect. These SW defected graphene flakes at the nanoscale had distinct molecular absorption spectrum characteristics. This study mainly focuses on low-energy modes (i.e., less than 5 eV), as shown below.

Figure 2 clearly shows that compared with the isolated SW defected graphene, an obvious enhancement is found on the optical absorption of the hybrid structure. As sketched in the inset of Fig. 2, these silver nanowire dimers are expected to serve as optical antennas, which effectively convert the incident light into plasmon oscillation. The optical response intensity of the hybrid structure was closely linked with the resonant frequency of the silver nanowires. Hence, we combined four different silver nanowires (i.e., Ag2, Ag3, Ag4, and Ag5) with the same SW defected graphene when we built the hybrid structures.

Figures 2(a)–(d) depict the absorption spectra of four kinds of hybrid structures, in which the number of silver particles increased when the excitation pulse polarized along the X-axis direction. According to the optical absorption spectrum, the resonant frequency of the hybrid structure gradually enhanced when the number of silver atoms on one side of the SW defected graphene increased from 2 to 5. The region of the low energy resonance absorption peak gradually red shifted from 2.51 eV to 1.41 eV with the increase of the silver particles. Furthermore, the absorption intensity increased from 23 (1/eV) to 40 (1/eV). The appearance of the strong absorption peak suggested that these patterns had the collective excitation feature. This enhancement of the selective light absorption was mainly caused by the coherent superposition effect of the plasmons in the hybrid structure. The carrier concentration for this hybrid structure enhanced. Part of the electrons will shift between the SW defected graphene and the silver nanowires when the SW defected graphene is put in the silver nanowire dimer. Furthermore, the silver nanowire plasmons were produced by the incident light excitation that enhanced with the electron silver pulsed magnetic field near the area. This kind of strong near field will directly stimulate the hole electron pair in the SW defected graphene. Notably, the

enhanced mode frequency was very close to the resonant frequency of the silver particles in the abovementioned four kinds of hybrid structure because very approximate frequencies between the SW defected graphene and the silver nanowires can meet the coherence resonance conditions of plasmon. Hence, the electrons in the two materials had a coherence resonance with the approximate resonance frequency, and the resulting coherent effect, which appeared at the absorption peak, will obviously enhance. Fang *et al.* demonstrated that the wavelength sensitivity of a graphene–antenna sandwich photodetector is limited by the resonant frequency of the antennas. Moreover, the antenna frequency was implemented by varying the size of the antennas in the device [43].

We calculated the induced charge density distribution at the resonant frequency for the hybrid structures to more clearly illustrate the resonance mechanism of these plasmons. Figure 3 shows the induced charge density distributions for the four hybrid structures at the energy resonance points. The charge was mainly concentrated at the edge of the hybrid position, thereby showing a very significant dipole distribution. The plasmons in the two kinds of materials resonated when the induced charge density presented the dipole oscillation characteristics between the SW defected graphene and the silver nanowires. In other words, the electromagnetic coupling that existed in the hybrid structure will form the antiparallel dipole. The experiment of Niu *et al.* proved that the electromagnetic coupling will be shown as the plasmon coherence resonance when the resonant frequency of the two is very close [44]. At this time, the current carriers of the SW defected graphene and the silver nanowires are oscillating in the same frequency. At the same time, the SW defected graphene–silver nanowires showed a dipole distribution in the induced charge density distribution corresponding to these energy points. The dipole interaction between the two led the resonance frequency of the plasmons in the system to the minimum mobile.

For a more intuitive comparison, Fig. 4 shows the induced charge density distributions of the isolated SW defected graphene at the energy resonance points. The isolated SW defected graphene can also take on the dipole oscillation characteristics to a certain extent. However, the overall distribution was scattered in terms of the charge density distribution. The effect of the silver nanowires was not difficult to find compared with the hybrid structure. The charge distribution was more concentrated; the dipole was significantly enhanced; and the light response degree obviously increased. The coherence resonance occurred between the silver nanowires and the SW defected graphene and can be regarded as a strong evidence.

In addition, the optical responses of this anisotropic hybrid structure were sensitively dependent on the space configuration of the hybrid structure. In this part, we tried to make some changes on the position between the silver nanowires and the SW defected graphene. As shown in Fig. 5, the SW defected graphene rotates for 90° and at the zigzag boundary parallel to the Y axis. The inset of Fig. 5 illustrates that the distance between

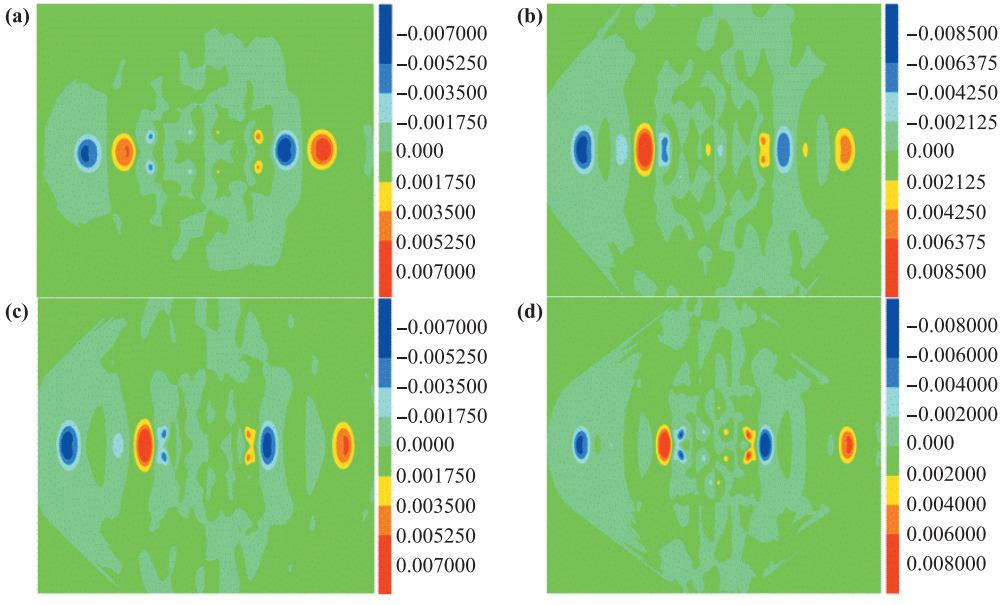

Fig. 3 The induced-charge-density distributions of the hybrid structures, **(a–d)** SW defected graphene-silver2/3/4/5 dimer, at the prominent resonance frequency of 2.51 eV/2.05 eV/1.62 eV/1.41 eV, respectively.

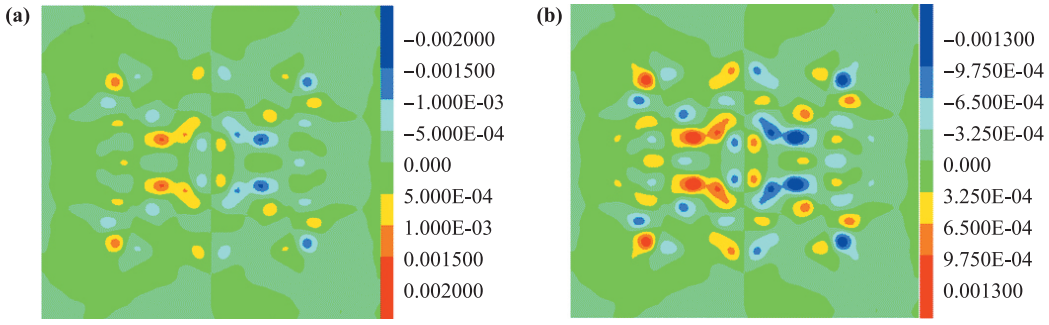

Fig. 4 The induced-charge-density distributions of the isolated SW defected graphene, **(a)** at the prominent resonance frequency of 1.41 eV, **(b)** at the prominent resonance frequency of 3.75 eV.

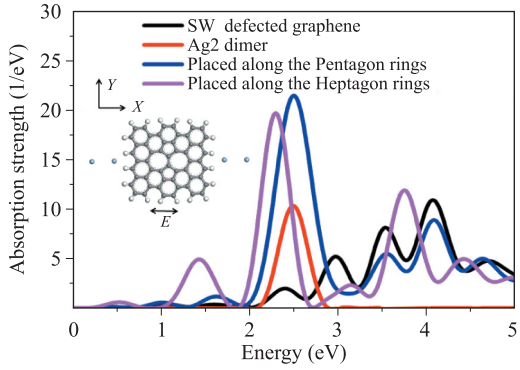

Fig. 5 The optical absorption spectrum of hybrid structure (Ag2 dimer placed along the heptagon rings) is displayed with a purple curve. For comparison, SW defected graphene is displayed with a black curve, isolated Ag2 dimer is displayed with a red curve, hybrid structure (Ag2 dimer placed along the pentagon rings) is displayed with a blue curve.

the nearest silver ions and the SW defected graphene was 2.6 Å. Figure 5 shows the optical absorption spectrum of the hybrid structure when the excitation light goes along the armchair-type edge of the SW defected graphene (parallel to the X axis).

Figure 5 clearly displays two obvious absorption peaks in the new hybrid structure at a low-energy area, which was not the same as before. The optical absorption of the new hybrid structure still had an obvious enhancement compared with the isolated defected graphene. However, a weaker hybrid structure than the former was observed in the highest absorption peak on the low-energy modes. The new hybrid structure also showed a coherent superposition effect of the plasmons. The hybrid structure can enhance the light absorption of the visible region compared with the isolated SW defected graphene. The electrons of the SW defected graphene and the silver nanowires exhibited a coherence resonance in the same frequency. The coherent superposition effect was characterized by the enhancement of the absorption peak in the light absorption spectrum. On the one hand, the current carrier concentration was an important factor to the strength of the light absorption spectrum because of the special structure of the SW defected graphene (i.e., four hexagon rings go into two pentagon and two heptagon rings). The atoms in the silver nanowire dimer were less when the silver nanowires were placed alongside the heptagon rings. On the other hand, this phenomenon can be attributed to the boundary effect of the defected graphene on nanoscale. The resonance absorption spectrum of the plasmons reflected the long-range oscillation transmission process of the charge under the action of Coulomb. In essence, the electron of the dimer transfer needed to experience different distances and barriers under the action of the excitation light when the coupling structure makes an adjustment. The absorption frequency and intensity in the two directions had a certain difference because the barrier and the Landau damping were different from the carrier oscillation along the armchair-shaped edges and the zigzag edge. Figure 6 shows the induced charge density distribution of the new hybrid structure at 1.41 eV and 2.25 eV to facilitate better understanding.

Figure 6 shows that the electrons that transferred between the silver nanowires and the SW defected graphene becomes less when the silver nanowires and the SW defected graphene are in a parallel or antiparallel dipole distribution. As can be seen from the induced charge density figure for defected graphene, different modes corresponded to different space charge distributions. Furthermore, the induced charge in the low-energy absorption model mainly focused on its edge. A scanning tunneling microscope (STM) is an instrument used for imaging surfaces at the atomic level. For an STM, a good resolution is considered to be 0.1 nm lateral resolution and 0.01 nm (10 pm) depth resolution. The individual atoms within the materials were routinely imaged and manipulated following this resolution. The boundary effect can

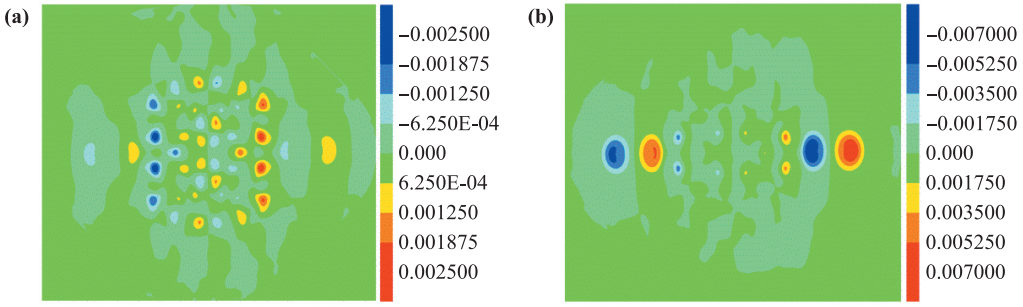

Fig. 6 The induced charge density distributions for the hybrid structure (Ag2 dimer placed along heptagon rings), **(a)** at the prominent resonance frequency of 1.41 eV, **(b)** at the prominent resonance frequency of 2.25 eV.

be directly observed by the STM and a scanning tunneling spectrum experiment [45]. The electronic structure under the boundary condition will produce a very big effect on the model and a light response of the SW defected graphene [46, 47]. The situation for the sheet structure of the small-scale rectangular defected graphene on the two kinds of boundary (i.e., zigzag and armchair boundaries) that we used in the calculation was more complicated.

We opted for a high-symmetry system consisting of a SW defected graphene flake and a silver nanowire tetramer to further confirm the view of the boundary effect and attain a better understanding of the physical essence of the resonance mode transformation. This hybrid structure exhibited excitation on the incident light with different reverse polarizations. Figure 7 shows the absorption spectrum of the special hybrid structure under the excitation from different polarized lights.

We found that the resonant frequency and intensity only had minor changes with the excitation light polarization direction in the low-energy region. Figure 7 also demonstrates that the SW defected graphene only had a single zigzag boundary, while the silver nanowire tetramer was placed symmetrically in the X and Y directions. The electron transferred in the same distance and barrier height along all directions only because of the single zigzag boundary in the SW defected graphene. Moreover, the silver nanowire tetramer was vertically stacked. Therefore, the oscillation pattern was the same as that in the two mutually vertical directions. In the process of model transformation, the coherence resonance condition was always met. The abovementioned analysis has carried on a rational explanation of the phenomenon that the light absorption of this kind of hybrid structure was basically not affected by the polarization direction of the excitation light in a low-energy region.

The following very interesting phenomenon deserves our attention: a new absorption peak in a low-energy zone gradually appears as the excitation light direction gradually changes. Combined with Fig. 7, the resonance frequency also depends on the space configuration of the

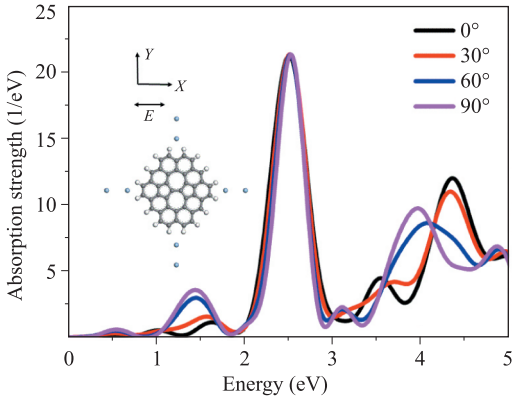

Fig. 7 Absorption spectra of a SW defected graphene–Ag2 nanowires tetramer hybrid structure as a function of the polarizer angle relative to the X axis ($\theta = 0°$, $30°$, $60°$, $90°$).

hybrid system. The obvious characteristics of the optical phenomena turned up in the low-energy region for two reasons. One is the influence of the boundary effect, and the other is related to the carrier concentration between the silver nanowire dimer and the SW defected graphene.

Figures 8(a)–(d) present the induced charge density distribution under the excitation of the polarized light in different directions. Figure 8 intuitively shows the oscillation mode conversion of the hybrid structure when the excitation light polarization direction increases from 0° to 90°. The SW defected graphene sheets and silver nanowires exhibited dipole phenomena under these four excitations of polarized light (i.e., 0°, 30°, 60°, 90°). This observation was enough to show that the coherence resonance of the hybrid structure happened. The transverse mode in this high symmetrical structure can increase accordingly when the longitudinal mode decreases. Meanwhile, the longitudinal mode can increase accordingly when the lateral pattern weakens. The vertical and horizontal enhancement patterns were trading off and taking turns, thereby resulting to the total absorption intensity remaining to be unchanged.

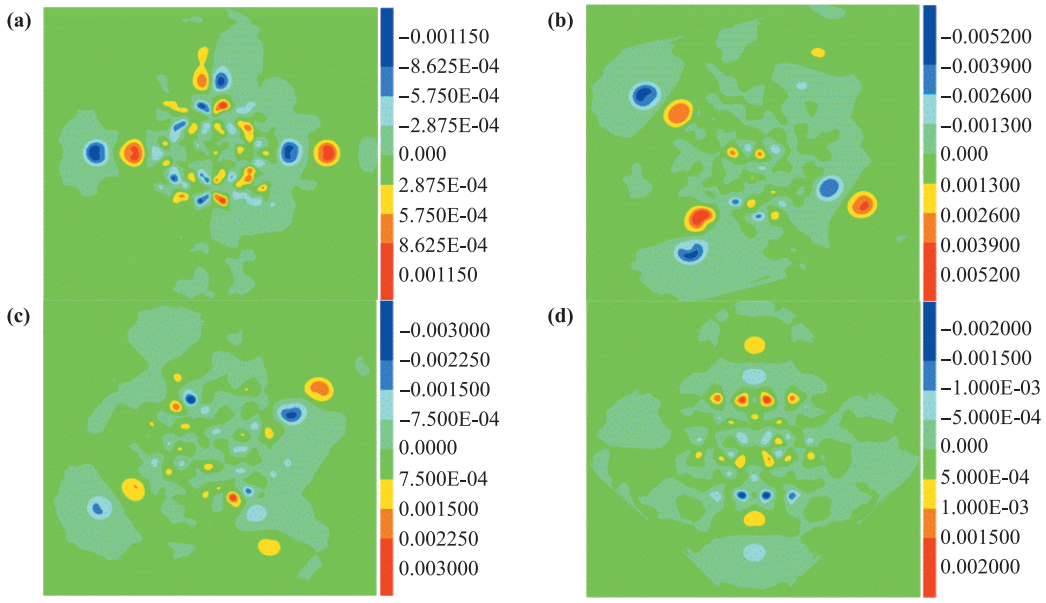

Fig. 8 The induced charge density distributions for the SW defected graphene–Ag2 nanowires tetramer hybrid structure at different polarizer angles. **(a)** 0°, **(b)** 30°, **(c)** 60°, **(d)** 90°.

4 Conclusion

In summary, our work provides the first detailed theoretical analysis of the plasmon coherent resonance in the SW defected graphene–silver nanowire hybrid system by using the time-dependent density functional theory.

We draw the following conclusions according to the abovementioned theoretical simulation of plasmons in the hybrid structure:

i) The quantum plasmon coherent effect in the Stone–Wales defected graphene–silver nanowire hybrid system can dramatically enhance the absorption in the visible light region. The absorption intensity is proportional to the length of the silver nanowires. Similarly, the absorption frequency is regulated by the silver nanowires.

ii) The plasmons in the hybrid structure are more easily tunable by changing the polarization direction because of the anisotropic edge effect in the SW defected graphene flake and mode conversion in a silver nanowire antenna. Moreover, they can eliminate the excitation light polarization direction of anisotropy to a certain extent using the high-symmetry hybrid structure. The conclusions provide a more effective strategy for a nanoscale plasmon device in the visible region. The findings also offer a feasible method of testing the existence of defects in graphene.

Acknowledgements We thank the financial support from the National Natural Science Foundation of China (Grant Nos. 11474207 and 11374217).

References

1. S. A. Maier and H. A. Atwater, Plasmonics: Localization and guiding of electromagnetic energy in metal/dielectric structures, *J. Appl. Phys.* 98(1), 011101 (2005)
2. A. Karalis, E. Lidorikis, M. Ibanescu, J. D. Joannopoulos, and M. Soljačić, Surface-plasmon-assisted guiding of broadband slow and subwavelength light in air, *Phys. Rev. Lett.* 95(6), 063901 (2005)
3. Y. C. Cao, R. Jin, and C. A. Mirkin, Nanoparticles with Raman spectroscopic fingerprints for DNA and RNA detection, *Science* 297(5586), 1536 (2002)
4. S. A. Maier, P. G. Kik, and H. A. Atwater, Observation of coupled plasmon-polariton modes in Au nanoparticle chain waveguides of different lengths: Estimation of waveguide loss, *Appl. Phys. Lett.* 81(9), 1714 (2002)
5. L. Novotny and N. Van Hulst, Antennas for light, *Nat. Photonics* 5(2), 83 (2011)
6. A. Gonzalez-Tudela, D. Martin-Cano, E. Moreno, L. Martin-Moreno, C. Tejedor, and F. J. Garcia-Vidal, Entanglement of two qubits mediated by one-dimensional plasmonic waveguides, *Phys. Rev. Lett.* 106(2), 020501 (2011)
7. W. Choi, I. Lahiri, R. Seelaboyina, and Y. S. Kang, Synthesis of graphene and its applications: A review, *Crit. Rev. Solid State Mater. Sci.* 35(1), 52 (2010)
8. F. J. Garcia de Abajo, Graphene nanophotonics, *Science* 339(6122), 917 (2013)
9. F. Schwierz, Graphene transistors, *Nat. Nanotechnol.* 5(7), 487 (2010)

10. L. Liao, Y. C. Lin, M. Bao, R. Cheng, J. Bai, Y. Liu, Y. Qu, K. L. Wang, Y. Huang, and X. Duan, High-speed graphene transistors with a self-aligned nanowire gate, *Nature* 467(7313), 305 (2010)
11. F. H. L. Koppens, D. E. Chang, and F. J. Garcia de Abajo, Graphene plasmonics: A platform for strong light-matter interactions, *Nano Lett.* 11(8), 3370 (2011)
12. A. Vakil and N. Engheta, Transformation optics using graphene, *Science* 332(6035), 1291 (2011)
13. S. Thongrattanasiri, F. H. L. Koppens, and F. J. Garcia de Abajo, Complete optical absorption in periodically patterned graphene, *Phys. Rev. Lett.* 108(4), 047401 (2012)
14. J. H. Chen, C. Jang, S. D. Xiao, M. Ishigamiand, and M. S. Fuhrer, Intrinsic and extrinsic performance limits of graphene devices on SiO_2, *Nat. Nanotechnol.* 3(4), 206 (2008)
15. K. S. Novoselov, A. K. Geim, S. V. Morozov, D. Jiang, et al., Electric field effect in atomically thin carbon films, *Science* 306(5696), 666 (2004)
16. C. C. Neacsu, J. Dreyer, N. Behr, and M. B. Raschke, Scanning-probe Raman spectroscopy with single-molecule sensitivity, *Phys. Rev. B* 73(19), 193406 (2006)
17. K. Zhang, H. Zhang, and C. Li, Coherent resonance of quantum plasmons in the graphene-gold cluster hybrid system, *Phys. Chem. Chem. Phys.* 17(18), 12051 (2015)
18. M. D. Sonntag, J. M. Klingsporn, L. K. Garibay, J. M. Roberts, J. A. Dieringer, T. Seideman, K. A. Scheidt, L. Jensen, G. C. Schatz, and R. P. Van Duyne, Single-molecule tip-enhanced Raman spectroscopy, *J. Phys. Chem. C* 116(1), 478 (2012)
19. E. M. van S. Lantman, T. Deckert-Gaudig, A. J. G. Mank, V. Deckert, and B. M. Weckhuysen, Catalytic processes monitored at the nanoscale with tip-enhanced Raman spectroscopy, *Nat. Nanotechnol.* 7(9), 583 (2012)
20. R. Zhang, Y. Zhang, Z. C. Dong, S. Jiang, C. Zhang, L. G. Chen, L. Zhang, Y. Liao, J. Aizpurua, Y. Luo, J. L. Yang, and J. G. Hou, Chemical mapping of a single molecule by plasmon-enhanced Raman scattering, *Nature* 498(7452), 82 (2013)
21. T. W. Ebbesen and T. Takada, Topological and SP^3 defect structures in nanotubes, *Carbon* 33(7), 973 (1995)
22. D. Wu, K. Yan, Y. Zhou, H. Wang, L. Lin, H. Peng, and Z. Liu, Plasmon-enhanced photothermoelectric conversion in chemical vapor deposited graphene p–n junctions, *Chem. Soc.* 135(30), 10926 (2013)
23. Y. Takatsuka, K. Takahagi, E. Sano, II Ryzh, and T. Otsuji, Gain enhancement in graphene terahertz amplifiers with resonant structures, *J. Appl. Phys.* 112(3), 033103 (2012)
24. Y. Liu, R. Cheng, L. Liao, H. Zhou, J. Bai, G. Liu, L. Liu, Y. Huang, and X. Duan, Plasmon resonance enhanced multicolour photodetection by graphene, *Nat. Commun.* 2, 579 (2011)
25. A. Ferreira and N. M. R. Peres, Complete light absorption in graphene-metamaterial corrugated structures, *Phys. Rev. B* 86(20), 205401 (2012)
26. Y. Li, H. Zhang, D. W. Yan, H. F. Yin, and X. L. Cheng, Secondary plasmon resonance in graphene nanostructures, *Front. Phys.* 10(1), 102 (2015)
27. G. Bachelier, I. Russier-Antoine, E. Benichou, C. Jonin, N. DelFatti, F. Vallee, and P. F. Brevet, Fano profiles induced by near-field coupling in heterogeneous dimers of gold and silver nanoparticles, *Phys. Rev. Lett.* 101(19), 197401 (2008)
28. L. V. Brown, H. Sobhani, J. B. Lassiter, P. Nordlander, and N. J. Halas, Heterodimers: Plasmonic properties of mismatched nanoparticle pairs, *ACS Nano* 4(2), 819 (2010)
29. T. G. Habteyes, S. Dhuey, S. Cabrini, P. J. Schuck, and S. R. Leone, Theta-shaped plasmonic nanostructures: Bringing "dark" multipole plasmon resonances into action via conductive coupling, *Nano Lett.* 11(4), 1819 (2011)
30. J. J. Mock, R. T. Hill, A. Degiron, S. Zauscher, A. Chilkoti, and D. R. Smith, Distance-dependent plasmon resonant coupling between a gold nanoparticle and gold film, *Nano Lett.* 8(8), 2245 (2008)
31. M. M. Miller and A. A. Lazarides, Lazari des, A, Sensitivity of metal nanoparticle surface plasmon resonance to the dielectric environment, *J. Phys. Chem. B* 109(46), 21556 (2005)
32. T. Pakizeh and M. Käll, Unidirectional ultracompact optical nanoantennas, *Nano Lett.* 9(6), 2343 (2009)
33. P. K. Jain and M. A. El-Sayed, Plasmonic coupling in noble metal nanostructures, *Chem. Phys. Lett.* 487(4–6), 153 (2010)
34. R. Zhang, Y. Zhang, Z. C. Dong, S. Jiang, C. Zhang, L. G. Chen, L. Zhang, Y. Liao, J. Aizpurua, Y. Luo, J. L. Yang, and J. G. Hou, Chemical mapping of a single molecule by plasmon-enhanced Raman scattering, *Nature* 498(7452), 82 (2013)
35. H. X. Xu, J. Aizpurua, M. Käll, and P. E. Apell, Electromagnetic contributions to single molecule sensitivity in surface-enhanced Raman scattering, *Phys. Rev. E* 62(3), 4318 (2000)
36. J. Stadler, T. Schmid, and R. Zenobi, Nanoscale chemical imaging using top-illumination tip-enhanced Raman Spectroscopy, *Nano Lett.* 10(11), 4514 (2010)
37. S. Yoshizawa, H. Kim, T. Kawakami, Y. Nagai, T. Nakayama, X. Hu, Y. Hasegawa, and T. Uchihashi, Imaging Josephson vortices on the surface superconductor Si(111)–($\sqrt{7}\times\sqrt{3}$)–In, *Phys. Rev. Lett.* 113(24), 247004 (2014)
38. M. A. L. Marques, A. Castro, G. F. Bertsch, and A. Rubio, Octopus: A first-principles tool for excited electron–ion dynamics, *Comput. Phys. Commun.* 151(1), 60 (2003)

39. N. Troullier and J. L. Martins, Efficient pseudopotentials for plane-wave calculations, *Phys. Rev. B* 43, 1993 (1991)
40. D. M. Ceperley and B. J. Alder, Ground state of the electron gas by a stochastic method, *Phys. Rev. Lett.* 45(7), 566 (1980)
41. J. Yan, Z. Yuan, and S. W. Gao, End and central plasmon resonances in linear atomic chains, *Phys. Rev. Lett.* 98(21), 216602 (2007)
42. D. C. Marinica, A. K. Kazansky, P. Nordlander, J. Aizpurua, and A. G. Borisov, Quantum plasmonics: Nonlinear effects in the field enhancement of a plasmonic nanoparticle dimer, *Nano Lett.* 12(3), 1333 (2012)
43. Z. Y. Fang, Z. Liu, Y. M. Wang, P. M. Ajayan, P. Nordlander, and N. J. Halas, Graphene-antenna sandwich photodetector, *Nano Lett.* 12(7), 3808 (2012)
44. J. Niu, Y. J. Shin, Y. Lee, J.-H. Ahn, and H. Yang, Graphene induced tunability of the surface plasmon resonance, *Appl. Phys. Lett.* 100(6), 061116 (2012)
45. Y. Kobayashi, K. Fukui, T. Enoki, K. Kusakabe, and Y. Kaburagi, Observation of zigzag and armchair edges of graphite using scanning tunneling microscopy and spectroscopy, *Phys. Rev. B* 71(19), 193406 (2005)
46. L. Brey and H. A. Fertig, Elementary electronic excitations in graphene nanoribbons, *Phys. Rev. B* 75(12), 125434 (2007)
47. Y. W. Son, M. L. Cohen, and S. G. Louie, Energy gaps in graphene nanoribbons, *Phys. Rev. Lett.* 97(21), 216803 (2006)